

Superconductivity in Chromium Nitrides $\text{Pr}_3\text{Cr}_{10-x}\text{N}_{11}$ with Strong Electron Correlations

Wei Wu^{1,2}, Kai Liu³, Yanjie Li^{1,2}, Zhenhai Yu⁴, Desheng Wu^{1,2}, Yuting Shao^{1,2},
Shihang Na^{1,2}, Gang Li^{1,5}, Ruizhen Huang^{2,6}, Tao Xiang^{1,2,6} & Jianlin Luo^{1,2,5,*}

¹Beijing National Laboratory for Condensed Matter Physics and Institute of Physics, Chinese Academy of Sciences, Beijing 100190, China

²School of Physical Sciences, University of Chinese Academy of Sciences, Beijing 100190, China

³Department of Physics and Beijing Key Laboratory of Opto-electronic Functional Materials & Micro-nano Devices, Renmin University of China, Beijing 100872, China

⁴School of Physical Science and Technology, ShanghaiTech University, Shanghai 201210, China

⁵Songshan Lake Materials Laboratory, Dongguan, Guangdong 523808, China

⁶Kavli Institute for Theoretical Sciences, Beijing 100190, China

*Correspondence should be addressed to J. L. Luo (jlluo@iphy.ac.cn)

ABSTRACT

Exploration of superconductivity in Cr-based compounds has attracted considerable interest because only few Cr-based superconductors (CrAs , $\text{A}_2\text{Cr}_3\text{As}_3$ and ACr_3As_3 ($\text{A} = \text{K}, \text{Rb}, \text{Cs}, \text{Na}$)) have been discovered so far and that they show unconventional pairing mechanism. We report the discovery of bulk superconductivity at 5.25 K in chromium nitride in $\text{Pr}_3\text{Cr}_{10-x}\text{N}_{11}$ with a cubic lattice structure. A relatively large upper critical field of $H_{c2}(0) \sim 12.6$ T is determined, which is larger than the estimated Pauli paramagnetic pair-breaking magnetic field. The material has a large electronic specific-heat coefficient of $170 \text{ mJ K}^{-2} \text{ mol}^{-1}$, about 10 times larger than that estimated by the electronic structure calculation, which suggests that correlations between 3d electrons is very strong in $\text{Pr}_3\text{Cr}_{10-x}\text{N}_{11}$, and thus quantum fluctuations might be involved. Electronic structure calculations show that the density of states at the Fermi energy is contributed predominantly by Cr 3d electrons, implying that the superconductivity results mainly from the condensation of Cr 3d electrons. $\text{Pr}_3\text{Cr}_{10-x}\text{N}_{11}$ represents a rare example that possibly unconventional

superconductivity emerges in a three-dimensional system with strong electron correlations. Nevertheless, clarification of the specific pairing symmetry needs more investigations.

Keywords: Cr-based Superconductors, Nitrides, Strong Electron Correlations, Unconventional Superconductivity.

INTRODUCTION

The 3d transition-metal oxides or pnictides exhibit rich quantum phases with novel quantum states, such as long-range magnetic orders, charge or spin density waves, metal-insulator transitions, high- T_c superconductivity, and colossal magnetoresistance. In particular, unconventional high- T_c superconductivity has been discovered in cuprates as well as in iron-based superconductors [1,2]. Many compounds with 3d transition-metal elements can become superconducting at low temperature. However, it is relatively difficult to find a superconducting material in chromium-based compounds because most Cr-based compounds have strong magnetism which generally is not in favor of superconductivity. In fact, CrAs, $A_2Cr_3As_3$ and ACr_3As_3 ($A = Na, K, Rb, Cs$) are the only Cr-based superconductors so far [3-6].

Superconductivity in CrAs was discovered in 2014 [3,4], CrAs undergoes a first-order antiferromagnetic transition with a double helical spin structure at $T_N \approx 265$ K [3,7,8]. A bulk superconductivity with $T_c \approx 2$ K emerges above a pressure $P_c \approx 8$ kbar, where the antiferromagnetic order is completely suppressed. Both the NMR and neutron scattering measurements for CrAs under high pressure revealed that there are strong magnetic fluctuations and line nodes may exist in the superconducting gap function [9-13], like in Sr_2RuO_4 or some heavy fermion superconductors [14,15]. After the discovery of superconductivity in CrAs, superconductivity has also been found in the quasi-one-dimensional compounds $A_2Cr_3As_3$ ($A = K, Rb, Cs$) [3,4]. The upper critical field H_{c2} of $K_2Cr_3As_3$ is about three times larger than the Pauli-paramagnetic limit.

In this paper, we report a novel Cr-based nitride superconductor with cubic structure, $Pr_3Cr_{10-x}N_{11}$, which was first synthesized and characterized by Broil *et al.* in 1995 [16]. The compound crystallizes in space group $Fm-3m$ (No. 225) with lattice constant $a = 12.891$ Å. It contains 192 atoms in a face-centered cubic (FCC) cell with

three kinds of building blocks as illustrated in Fig. 1 (a). The building blocks are Pr_6N_9 , Cr_8N_{13} and Cr_6 . Previous studies showed that there are Cr vacancies in the lattice structure. However, no low temperature physical properties were reported [16,17]. Our key finding of this study is the observation of superconductivity in $\text{Pr}_3\text{Cr}_{10-x}\text{N}_{11}$ with $T_c \sim 5.25$ K. The high quality samples have a shielding fraction of 85% at 2 K from zero-field-cooled (ZFC) magnetic susceptibility and a prominent superconducting peak in specific heat measurement. A relatively large upper critical field is found at the zero-temperature limit, $H_{c2}(0) \sim 12.6$ T, which is larger than the Pauli paramagnetic pair-breaking field. From electronic structure calculations, we find that the density of states at the Fermi energy are predominately contributed by Cr 3d electrons. The present results demonstrate that $\text{Pr}_3\text{Cr}_{10-x}\text{N}_{11}$ is the first Cr-based superconductor discovered in Chromium Nitrides and it represents a rare example that possibly unconventional superconductivity emerges in a 3D system with strong electron correlations.

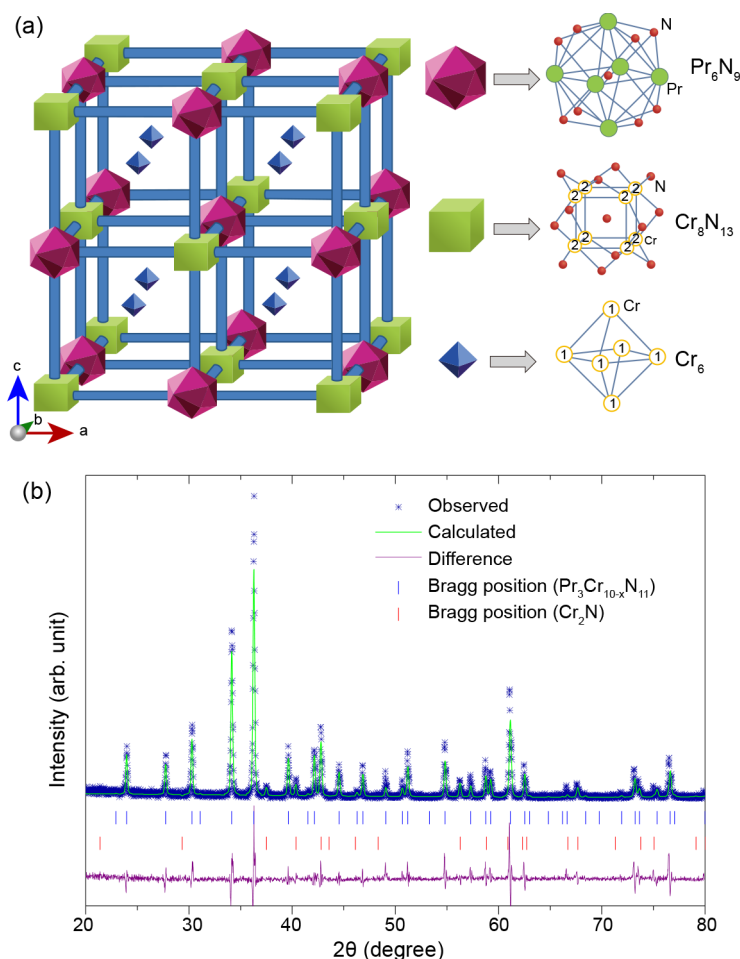


Figure 1. (a) The face-centered cubic cell of $\text{Pr}_3\text{Cr}_{10-x}\text{N}_{11}$ with three kinds of building blocks Pr_6N_9 , Cr_8N_{13} and Cr_6 , respectively. The blocks are shown in a shrunken form. There are two Cr positions Cr1 and Cr2. (b) Typical Rietveld refinement of $\text{Pr}_3\text{Cr}_{10-x}\text{N}_{11}$ under ambient conditions.

The vertical bars represent the calculated Bragg reflection positions of the diffraction peaks for $\text{Pr}_3\text{Cr}_{10-x}\text{N}_{11}$. The difference between the observed (scatters) and the fitted patterns (line) is shown at the bottom of the diffraction peaks.

RESULTS AND DISCUSSION

Sample and characterization

Polycrystalline samples of $\text{Pr}_3\text{Cr}_{10-x}\text{N}_{11}$ samples were prepared by direct reactions of the corresponding binary nitrides with solid reaction. Synthesized powder shows a dark brown color and is air sensitive, as it is easily oxidized to Pr_2O_3 within few hours. **Figure 1(b)** shows the GSAS refinement of $\text{Pr}_3\text{Cr}_{10-x}\text{N}_{11}$ under ambient conditions, which indicates that $\text{Pr}_3\text{Cr}_{10-x}\text{N}_{11}$ crystallized in FCC structure with space group $Fm-3m$. All the $\text{Pr}_3\text{Cr}_{10-x}\text{N}_{11}$ reflections can be well indexed based on a cubic cell with lattice parameter $a = 12.8521 \text{ \AA}$, which is consistent with those reported in the literature ($a = 12.891 \text{ \AA}$) [16], indicating their ideal composition. A small amount of raw reactant Cr_2N was marked with red vertical bar.

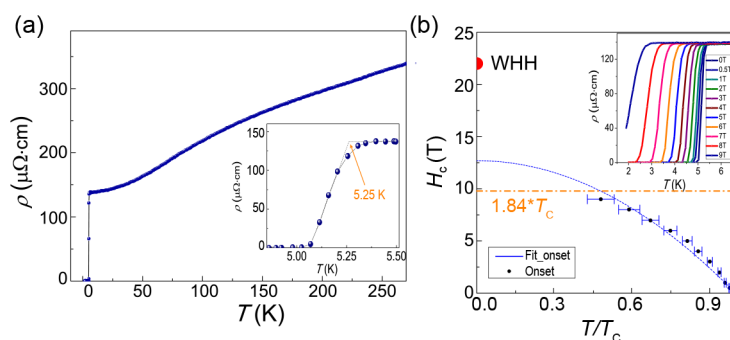


Figure 2. (a) Temperature dependence of the resistivity for $\text{Pr}_3\text{Cr}_{10-x}\text{N}_{11}$ from 1.8 K to 300 K at zero field. The inset shows the resistivity near superconducting transition. (b) The temperature dependence of the upper critical magnetic field. The solid circle shows the upper critical field obtained from WHH fitting. The inset shows temperature dependence of the resistivity at different fields.

Temperature dependent resistivity in $\text{Pr}_3\text{Cr}_{10-x}\text{N}_{11}$

Figure 2(a) shows the temperature dependent resistivity for $\text{Pr}_3\text{Cr}_{10-x}\text{N}_{11}$ from 1.8 K to 300 K at zero field. The normal state resistivity is metallic, with no phase transition observed. At low temperatures, a sharp superconducting transition is observed with onset T_c of about 5.25 K, as shown in the inset of **Fig. 2(a)**. The T_c of $\text{Pr}_3\text{Cr}_{10-x}\text{N}_{11}$ is higher than that of CrAs with $T_{max} \sim 2 \text{ K}$ under pressure, and is close to $\text{K}_2\text{Cr}_3\text{As}_3$ with $T_c \sim 6.1 \text{ K}$ [12].

The new superconductor $\text{Pr}_3\text{Cr}_{10-x}\text{N}_{11}$ shows a relatively large upper critical field. **Figure 2(b)** shows resistivity data in magnetic fields up to 9 T. As the field increases,

the transition temperature T_c shifts to lower temperature and the transition width is gradually broadened, similar to the iron-based superconductors [18,19]. The upper critical field H_{c2} (T) curve obtained from the field-dependent transition temperatures shows a remarkably high critical field of 12.6 T using the formula $H_{c2}(T) = H_{c2}(0)(1 - t^2)$, where t is the reduced temperature $t = T/T_c$ and of 22 T using the Werthamer–Helfand–Hohenberg (WHH) theory [20]. On the other hand, the Pauli paramagnetic limit for the upper critical field is $H_p = 1.84T_c \approx 9.6$ T in the case of isotropic full superconducting gap without considering spin-orbit coupling [21,22]. The $H_{c2}(0)$ in $\text{Pr}_3\text{Cr}_{10-x}\text{N}_{11}$ is 130% as large as H_p . Usually, the high superconducting upper critical field can be originated from multi-bands effects, the strong coupling effect, the spin-triplet pairing, and the strong spin–orbit coupling effect in low dimensional system [23–25]. The origin of large $H_{c2}(0)$ in $\text{Pr}_3\text{Cr}_{10-x}\text{N}_{11}$ need to be further studied. The obtained $\mu_0 H_{c2}(0)$ allows us to estimate the Ginzburg-Landau coherence length $\xi = 51$ Å according to the relationship: $\mu_0 H_{c2}(0) = \Phi_0 / 2\pi\xi^2$, where $\Phi_0 = 2.067 \times 10^{-15}$ Wb is the magnetic flux quantum.

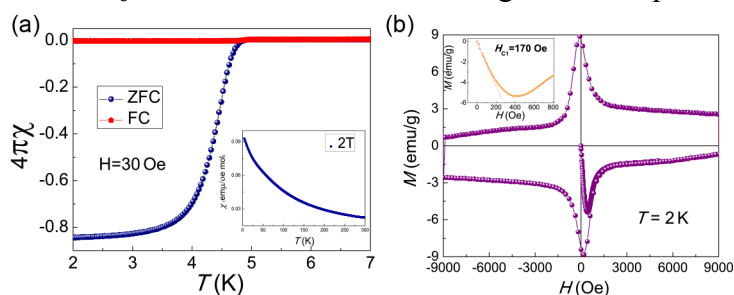


Figure 3. (a) Temperature dependence of the dc magnetic susceptibility with zero field cool (ZFC) and field cool (FC) measured in a field of 30 Oe. The inset of Fig. 3(a) is the normal state susceptibility measured in a field of 2 T. (b) The magnetic hysteresis of the sample measured at 2 K. The left inset shows the lower critical magnetic field.

Magnetic susceptibility measurements in $\text{Pr}_3\text{Cr}_{10-x}\text{N}_{11}$

The bulk superconductivity in $\text{Pr}_3\text{Cr}_{10-x}\text{N}_{11}$ was confirmed by magnetic susceptibility measurements. Figure 3(a) shows susceptibility χ at low temperature with zero field cool (ZFC) and field cool (FC) under a magnetic field of 30 Oe. χ starts to drop below T_c and the diamagnetic signal tends to saturate at low temperatures. The shielding fraction estimated from the ZFC magnetic susceptibility at 2 K is 85%, confirming bulk superconductivity in the sample. The normal state susceptibility χ increases with decreasing temperature in $\text{Pr}_3\text{Cr}_{10-x}\text{N}_{11}$, showing a Curie-Weiss behavior as shown in inset of Fig.3(a). Such a behavior is different from that of isostructural material $\text{La}_3\text{Cr}_{10-x}\text{N}_{11}$ which shows a Pauli paramagnetism with nearly a temperature-independent susceptibility [16]. Since La^{3+} ion has no occupied 4f electrons while each Pr^{3+} ion has 2 occupied 4f electrons, it is natural to attribute

the Curie-Weiss behavior of $\chi(T)$ in $\text{Pr}_3\text{Cr}_{10-x}\text{N}_{11}$ to the magnetic moments of Pr^{3+} 4f electrons. Using a Curie-Weiss fit with formula $\chi(T) = \chi_0 + C/(T-\theta)$, we obtained the effective moment of each Pr ion is about $3.6 \mu_B$, which is very close to the calculated moment of $3.5 \mu_B$ for Pr^{3+} by Hund's rule. The negative value of θ indicating the correlations between Pr ions are antiferromagnetic.

Further confirmation of superconductivity is shown by the magnetic hysteresis of the sample measured at 2 K in Fig. 3(b), which displays the typical magnetic hysteresis curve for a type-II superconductor. From the inset of Fig. 3(b), the lower critical magnetic fields H_{c1} of 170 Oe can be obtained.

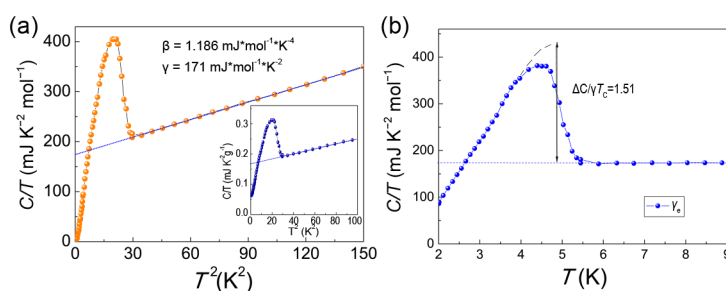


Figure 4. (a) The specific heat coefficient C/T of $\text{Pr}_3\text{Cr}_{10-x}\text{N}_{11}$ as a function of T^2 . The inset shows C/T versus T^2 for a sample with Cr_2N . (b) Temperature dependence of normalized electronic specific heat C_e/T .

Specific heat measurements

Figure 4(a) shows the specific heat coefficient C/T as a function of T^2 from 2 K to 10 K at zero field. The bulk nature of superconductivity is confirmed by a pronounced anomaly around $T_c = 5.25$ K, consistent with the resistivity and susceptibility measurements. Extrapolating C/T to zero temperature gives a residual value of $\gamma_0 = 0.061 \text{ mJ/g.K}^2$. As indicated previously, there is raw reactant phase Cr_2N in the sample. We measured specific heat of Cr_2N and found it can be well fitted by $C = \gamma T + \beta T^3$ below 10 K with $\gamma = 22 \text{ mJ/mol.K}^2$ and $\beta = 0.0373 \text{ mJ/mol.K}^4$. Given the residual specific heat γ_0 origin from the Cr_2N phase, we can then obtain specific heat of pure $\text{Pr}_3\text{Cr}_{10-x}\text{N}_{11}$ by subtracting that of Cr_2N from the total specific heat as shown in inset of Fig. 4(a).

Above T_c , the good linear T^2 dependence of C/T indicates that the normal state specific heat consists of two parts of contributions, the electronic part which is proportional to T and the phonon part which is proportional to T^3 at low temperatures. By fitting the normal state specific heat C with the formula $C = \gamma_n T + \beta T^3$, we find that $\gamma_n = 173 \text{ mJ K}^{-2} \text{ mol}^{-1}$. and $\beta = 1.186 \text{ mJ K}^{-4} \text{ mol}^{-1}$. The normal state electronic coefficient γ_n is proportional to the density of states at the Fermi level. Assuming that most of density of states come from the Cr 3d electrons, the value of γ_n per mole Cr is

$\gamma_n = 17.3 \text{ mJ K}^{-2} \text{ molCr}^{-1}$ for $\text{Pr}_3\text{Cr}_{10-x}\text{N}_{11}$, which is much larger than the corresponding value for CrAs ($\sim 7 \text{ mJ K}^{-2} \text{ mol}^{-1}$) and MnP ($\sim 8.3 \text{ mJ K}^{-2} \text{ mol}^{-1}$) at ambient pressure [11,26], and it is slightly less than that for $\text{K}_2\text{Cr}_3\text{As}_3$ ($\sim 23.3 \text{ mJ K}^{-2} \text{ molCr}^{-1}$) and KCr_3As_3 ($\sim 27.1 \text{ mJ K}^{-2} \text{ molCr}^{-1}$) [14,27,28]. The relatively large γ_n for $\text{Pr}_3\text{Cr}_{10-x}\text{N}_{11}$ indicates strong correlations of Cr 3d electrons. The Debye temperature θ_D obtained from β is 339 K.

In Fig. 4(b), the normalized specific heat jump at T_c is found to be $\Delta C/\gamma_n T_c = 1.51$. This value is much smaller than those of $\text{K}_2\text{Cr}_3\text{As}_3$ (~ 2.5) and LaNiAsO (~ 1.9), which are regarded as strong-coupling superconductivity [14,27,29]. The normalized $\Delta C/\gamma_n T_c$ reflects coupling strength between the conducting electrons and pairing glue. We can then estimate the electron-phonon coupling constant $\lambda = 0.6$ from the modified McMillan formula [25,30,31].

$$\lambda = \frac{1.04 + \mu^* \ln(\omega/1.2T_c)}{(1 - 0.62\mu^*) \ln(\omega/1.2T_c) - 1.04}$$

where μ^* is a Coulomb pseudopotential and ω is a logarithmic averaged phonon frequency. ω can be determined from the specific heat jump at T_c using the formula: $\Delta C/\gamma_n T_c = 1.43[1 + 53(T_c/\omega)^2 \ln(\omega/3T_c)]$. Taking $\mu^* = 0.10$ and $T_c = 5.25 \text{ K}$, we obtained $\omega = 320 \text{ K}$ and $\lambda = 0.6$. For such a small electron-phonon coupling constant, the large $H_{c2}(0)$ value is not likely due to the strong coupling effect.

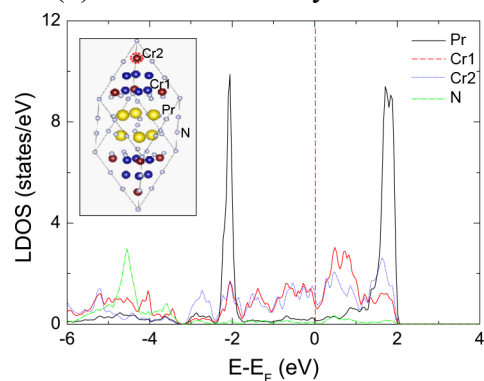


Figure 5. Local density of states (LDOS) for Pr, Cr1, Cr2, and N atoms in $\text{Pr}_3\text{Cr}_{9.5}\text{N}_{11}$. Inset shows a primitive cell with the yellow, blue, maroon, and gray balls representing Pr, Cr1, Cr2, and N atoms, respectively. The atomic vacancy at the Cr2 site is highlighted by a red dashed circle.

Theoretical calculations

In order to examine which atomic species contribute most around the Fermi level (E_F), we have plotted the local density of states (LDOS) for $\text{Pr}_3\text{Cr}_{9.5}\text{N}_{11}$ as shown in Fig. 5. Electronic structure calculations show that the density of states at the Fermi energy is contributed predominantly by Cr 3d electrons, implying that the superconductivity results mainly from the condensation of Cr 3d electrons similar to

that in CrAs [32]. The primitive cell of $\text{Pr}_3\text{Cr}_{10-x}\text{N}_{11}$ is shown in inset of Fig. 5, in which there are two types of nonequivalent Cr atoms, labeled as Cr1 and Cr2, respectively. Both the Cr1 and Cr2 atoms have large contributions around E_F , mainly originating from the $3d$ orbitals of Cr atoms. In contrast, the vast majority of states for Pr and N atoms are far away from the Fermi level. A higher density of Cr2 vacancies, such as in $\text{Pr}_3\text{Cr}_9\text{N}_{11}$, does not change the results very much. According to our calculations, the total DOS of $\text{Pr}_3\text{Cr}_{9.5}\text{N}_{11}$ at the Fermi level $N(E_F)$ is 7.37 states/(eV*f.u.). As a result, the corresponding calculated electronic specific-heat coefficient γ_e is $17.4 \text{ mJ K}^{-2} \text{ mol}^{-1}$. Experimentally, the measured γ_e for $\text{Pr}_3\text{Cr}_{10-x}\text{N}_{11}$ is about $173 \text{ mJ K}^{-2} \text{ mol}^{-1}$, about 10 times more than the band calculations, which indicates the strong mass enhancement effect.

CONCLUSIONS

Superconductivity in $\text{Pr}_3\text{Cr}_{10-x}\text{N}_{11}$ shows several novel characters. First, electronic structure calculations show that most of density of states at Fermi energy is contributed by Cr $3d$ electrons, suggesting the superconductivity is originated from the condensation of Cr $3d$ electrons. So $\text{Pr}_3\text{Cr}_{10-x}\text{N}_{11}$ is the first Cr based superconductor discovered in nitrides. Other known few Cr-based superconductors (CrAs, $\text{A}_2\text{Cr}_3\text{As}_3$ and ACr_3As_3 ($A = \text{K, Rb, Cs, Na}$)) are arsenide. Superconductivity in CrAs emerges in the vicinity of a quantum critical point (QCP), and antiferromagnetic spin fluctuations associated with the quantum criticality could act as an important glue medium for Cooper pairing. Superconductivity in the quasi-one-dimensional compounds $\text{A}_2\text{Cr}_3\text{As}_3$ ($A = \text{K, Rb, Cs}$) shows non-s-wave pairing. Both of them show unconventional pairing mechanism. So the Cr d-electrons play an important role in electron correlations and possibly unconventional superconductivity in $\text{Pr}_3\text{Cr}_{10-x}\text{N}_{11}$ with Cr d electrons.

Second, $\text{Pr}_3\text{Cr}_{10-x}\text{N}_{11}$ has a relatively large upper critical field $H_{c2}(0) \sim 12.6 \text{ T}$, exceeding the Pauli limit of paramagnetic pair-breaking field, this is rare in three-dimensional structure superconductors, The upper critical field provides very important information on the superconducting pairing. This behavior resembles that unconventional superconducting in $\text{K}_2\text{Cr}_3\text{As}_3$ which H_{c2} is three times the Pauli-paramagnetic limit that is regarded as evidence of spin-triplet superconductivity.

Last but not the least, the measured γ_e for $\text{Pr}_3\text{Cr}_{10-x}\text{N}_{11}$ is about 173 mJ/mol K^2 , equivalent to $17.3 \text{ mJ K}^{-2} \text{ mol}(\text{Cr})^{-1}$. This γ value is close to that of $\text{K}_2\text{Cr}_3\text{As}_3$ ($\text{mJ K}^{-2} \text{ mol}(\text{Cr})^{-1}$) indicating enhanced electron correlations in $\text{Pr}_3\text{Cr}_{10-x}\text{N}_{11}$. The experimental of γ_e about 10 times more than the electronic calculations. This large renormalization

factor cannot be explained by electron-phonon interactions, and thus quantum fluctuations might be involved.

In conclusion, we report the experimental result for a novel Cr-based superconductor nitrides $\text{Pr}_3\text{Cr}_{10-x}\text{N}_{11}$ with cubic lattice structure. Bulk superconductivity with $T_c \sim 5.25$ K is observed from the resistivity, susceptibility, and specific heat measurements. Further theoretical and experimental studies are needed to determine the pairing symmetry and the corresponding mechanism, especially the role of Cr 3d electrons, for the observed superconductivity in $\text{Pr}_3\text{Cr}_{10-x}\text{N}_{11}$.

Methods

Sample preparation

Polycrystalline samples of $\text{Pr}_3\text{Cr}_{10-x}\text{N}_{11}$ were prepared by direct reactions of the corresponding binary nitrides, starting with PrN(99%) and a mixture of the chromium nitrides (CrN and Cr_2N) in a mass ratio of 4:6. The operations were all performed in Ar-filled glovebox. Cold-pressed pellets of the mixtures were sealed in an evacuated quartz tube ($< 10^{-4}$ Pa). The pellets were gradually heated in 1 day to 1000 °C, held at that temperature for 50 hours, then cooled to the room temperature in furnace. The products were again ground in glovebox, pressed into pellets, wrapped in Ta foil, and heated in evacuated quartz tube at 1165 °C for 120 hours. It is worth noting that after this treatment the samples were usually still contaminated by the binary nitrides. The treatment of these samples with diluted hydrochloric acid only dissolved the rare earth nitrides. In between these treatments the pellets were ground to a fine powder, the decomposed rare earth nitride was dissolved in hydrochloric acid and fresh rare earth nitride was added again to the mixture to maintain the proper composition. The reaction temperature was carefully selected to avoid decomposition of the products, meanwhile obtaining a good crystallization. In our study, we found that $\text{Pr}_3\text{Cr}_{10-x}\text{N}_{11}$ partially decomposed above 1200 °C. Synthesized powder shows a dark brown color and is air sensitive, as it is easily oxidized to Pr_2O_3 within few hours.

Measurements

The electrical transport measurement was carried out on a physical property measurement system (PPMS-9, Quantum Design). The resistivity was measured by a standard four probe method, employing silver paste contacts cured at room temperature, was used for resistivity measurements, with the electric current applied in an arbitrary direction. The magnetic susceptibility was measured in a Quantum Design SQUID VSM. The specific heat measurements were performed up to 9 T in a PPMS.

Theoretical modeling

We have carried out first-principles electronic structure calculations on $\text{Pr}_3\text{Cr}_{10-x}\text{N}_{11}$. The first-principles calculations were performed by using the projector augmented wave (PAW) method [33], as implemented in the VASP package [34]. The generalized gradient approximation (GGA) of Perdew-Burke-Ernzerhof (PBE) type [35] was adopted for the exchange-correlation functional.

SUPPLEMENTARY DATA

Supplementary data are available at NSR online.

ACKNOWLEDGEMENT:

The authors are grateful to Dr. Zhao Yu Liu and Prof. Shi Liang Li (Institute of Physics) for their help in experiments.

FUNDING

This work was supported by the National Basic Research Program of China (2017YFA0302901, 2014CB921500), the National Natural Science Foundation of China (11674375, 11634015), the Strategic Priority Research Program and Key Research Program of Frontier Sciences of the Chinese Academy of Sciences (XDB07020200).

References

- (1) Bednorz JG and Müller KZ. Possible high T_c superconductivity in the Ba–La–Cu–O system. *Z Phys B - Condens Mat* 1986; **64**: 189-93.
- (2) Kamihara Y, Watanabe T and Hirano M et al. Iron-Based Layered Superconductor $\text{La}[\text{O}_{1-x}\text{F}_x]\text{FeAs}$ ($x = 0.05\text{--}0.12$) with $T_c = 26$ K. *J Am Chem Soc* 2008; **130**: 3296-7.
- (3) Wu W, Cheng JG and Matsubayashi K et al. Superconductivity in the vicinity of antiferromagnetic order in CrAs. *Nat Commun* 2014; **5**:5508.
- (4) Kotegawa H, Nakahara S and Tou H et al. Superconductivity of 2.2 K under Pressure in Helimagnet CrAs. *J. Phys. Soc. Jpn* 2014; **83**: 238-41.
- (5) Bao J K, Liu JY and Ma CW et al. Superconductivity in Quasi-One-Dimensional $\text{K}_2\text{Cr}_3\text{As}_3$ with Significant Electron Correlations *Phys Rev X* 2015; **5**: 5568–77.
- (6) Tang ZT, Bao JK and Liu Y et al. Unconventional superconductivity in quasi-one-dimensional $\text{Rb}_2\text{Cr}_3\text{As}_3$. *Phys Rev B* 2015; **91**:020506; Tang ZT, Bao JK and Wang Z et al. Superconductivity in quasi-one-dimensional $\text{Cs}_2\text{Cr}_3\text{As}_3$ with large interchain distance. *Sci China Mater* 2015; **58**: 16-20; Mu QG, Ruan BB and Pan BJ, et al. Superconductivity at 5 K in quasi-one-dimensional Cr-based KCr_3As_3 single crystals. *Phys Rev B* 2017; **96**:140504; Liu T, Mu QG and Pan BJ et al. Superconductivity at 7.3 K in 133- type Cr-based RbCr_3As_3 single crystals. *Europhys Lett* 2017; **120**:27006.
- (7) Cheng JG, Matsubayashi K and Wu W et al. Pressure Induced Superconductivity on the border of Magnetic Order in MnP. *Phys Rev Lett* 2015; **114**:117001.
- (8) Cheng JG and Luo JL, Special issue on pressure-induced superconductivity in CrAs and MnP, *J Phys Condens Matter* 2017; **29**:440301.
- (9) Kotegawa H, Nakahara S and Akamatsu R et al. Detection of an Unconventional Superconducting Phase in the Vicinity of the Strong First-Order Magnetic Transition in CrAs Using ^{75}As -Nuclear Quadrupole Resonance. *Phys Rev Lett* 2015; **114**, 117002.
- (10) Keller L, White JS and Frontzek M et al. Pressure dependence of the magnetic

- order in CrAs: A neutron diffraction investigation. *Phys Rev B* 2015; 91:020409.
- (11) Shen Y, Wang QS and Hao YQ et al. Structural and magnetic phase diagram of CrAs and its relationship with pressure-induced superconductivity. *Phys Rev B* 2016; 93:060503.
- (12) Matsuda M, Ye F and Dissanayake SE et al. Pressure dependence of the magnetic ground states in MnP. *Phys Rev B* 2016; 93:100405.
- (13) Matsuda M, Lin FK and Yu R et al. Evolution of Magnetic Double Helix and Quantum Criticality near a Dome of Superconductivity in CrAs. *Phys Rev X* 2018; 8:031017.
- (14) Mackenzie AP, Haselwimmer RK W and Tyler AW et al. Extremely Strong Dependence of Superconductivity on Disorder in Sr_2RuO_4 . *Phys Rev Lett* 1998; 80:161-4.
- (15) Mathur ND, Grosche FM and Julian SR et al. Magnetically mediated superconductivity in heavy fermion compounds. *Nature* 1998; 394: 39-43.
- (16) Broil S and Jeitschko W et al. The Ternary Rare Earth Chromium Nitrides Ce_2CrN_3 and $\text{Ln}_3\text{Cr}_{10-x}\text{N}_{11}$ with $\text{Ln} = \text{La, Ce, Pr}$. *Z. Naturforsch B* 1995. 50b: 905-12.
- (17) Chevire F, Ranjan C and Disalvo F, Synthesis, crystal and electronic structures of $\text{La}_3\text{Cr}_2\text{N}_6$. *Solid State Commun* 2009; 149 (7-8):273-6.
- (18) Chen GF, Li Z and Li G et al. Superconducting Properties of the Fe-Based Layered Superconductor $\text{LaFeAsO}_{0.9}\text{F}_{0.1-\delta}$. *Phys Rev Lett* 2008; 101: 057007.
- (19) Chen GF, Li Z and Wu D et al. Superconductivity at 41 K and Its Competition with Spin-Density-Wave Instability in Layered $\text{CeO}_{1-x}\text{F}_x\text{FeAs}$. *Phys Rev Lett* 2008; 100:247002.
- (20) Werthamer N R and Helfand E. Temperature and Purity Dependence of the Superconducting Critical Field, H_{c2} . *Phys Rev Lett* 1964; 13: 686-8.
- (21) Clogston, A M. Upper Limit for the Critical Field in Hard Superconductors. *Phys Rev Lett* 1962. 9, 266-7
- (22) Chandrasekhar B S. A note on the maximum critical field of high-field superconductors. *Appl Phys Lett* 1962; 1: 7-8.
- (23) Gurevich A. Enhancement of the upper critical field by nonmagnetic impurities

- in dirty two-gap superconductors. *Phys Rev B* 2003; **67**:184515.
- (24) Carbotte,JP. Properties of boson-exchange superconductors. *Rev Mod Phys* 1990; **62**:1027- 158.
- (25) Lee IJ, Chaikin PM and Naughton MJ. Exceeding the Pauli paramagnetic limit in the critical field of (TMTSF)₂PF₆. *Phys Rev B* 2000; **62**: 14669-72.
- (26) Zheng P, Xu YJ and Wu W et al. Orbital-dependent charge dynamics in MnP revealed by optical study. *Sci Rep* 2017; **7**: 14178.
- (27) Shao YT, Wu XX and Wang L et al. Evidence of line nodes in superconducting gap function in K₂Cr₃As₃ from specific-heat measurements. *Europhys Lett* 2018; **123**: 57001.
- (28) Mu QG, Ruan BB and Pan BJ et al. Dynamic instabilities in strongly correlated VSe₂ monolayers and bilayers. *Phys Rev B* 2017; **96**: 140524.
- (29) Li Z, Chen GF and Dong J et al. Strong-coupling superconductivity in the nickel-based oxypnictide LaNiAsO_{1-x}F_x. *Phys Rev B* 2008; **78**: 060504.
- (30) Allen P B and Dynes R C. Transition temperature of strong-coupled superconductors reanalyzed. *Phys Rev B* 1975;**12**: 905-22.
- (31) Klimczuk T, Ronning F and Sidorov V et al. Physical Properties of the Noncentrosymmetric Superconductor Mg₁₀Ir₁₉B₁₆. *Phys Rev Lett* 2007; **99**: 257004.
- (32) Autieri C and Noce C. First principles study of structural, magnetic and electronic properties of CrAs. *Philos Mag* 2017; **97**: 3276-95.
- (33) Blöchl PE. Projector augmented-wave method. *Phys Rev B* 1994; **50**: 17953-17979; Kresse G and Joubert D. From ultrasoft pseudopotentials to the projector augmented-wave method. *Phys Rev B* 1999; **59**: 1758-1775.
- (34) Kresse G and Hafner J. *Ab initio* molecular dynamics for liquid metals. *Phys Rev B* 1993; **47**: 558-561; Kresse G and Furthmüller J. Efficiency of ab-initio total energy calculations for metals and semiconductors using a plane-wave basis set. *Comp Mater Sci* 1996; **6**: 15-50; Kresse G and Furthmüller J. Efficient iterative schemes for *ab initio* total-energy calculations using a plane-wave basis set. *Phys Rev B* 1996; **54**: 11169-11186.
- (35) Perdew JP, Burke K and Ernzerhof M. Generalized gradient approximation made simple. *Phys Rev Lett* 1996; **77**, 3865-3868.